crystals

MDPI

Article

In Situ Random Microseeding and Streak Seeding Used for Growth of Crystals of Cold-Adapted β-D-Galactosidases: Crystal Structure of βDG from *Arthrobacter* sp. 32cB

Maria Rutkiewicz-Krotewicz [1], Agnieszka J. Pietrzyk-Brzezinska [1], Marta Wanarska [2], Hubert Cieslinski [2] and Anna Bujacz [1,*]

[1] Institute of Technical Biochemistry, Faculty of Biotechnology and Food Sciences, Lodz University of Technology, Stefanowskiego 4/10, 90-924 Lodz, Poland; maria.rutkiewicz-krotewicz@dokt.p.lodz.pl (M.R.-K.); agnieszka.pietrzyk-brzezinska@p.lodz.pl (A.J.P.-B.)

[2] Department of Molecular Biotechnology and Microbiology, Faculty of Chemistry, Gdansk University of Technology, Narutowicza 11/12, 80-233 Gdansk, Poland; marta.wanarska@pg.edu.pl (M.W.); hubert.cieslinski@pg.edu.pl (H.C.)

* Correspondence: anna.bujacz@p.lodz.pl

Received: 29 November 2017; Accepted: 29 December 2017; Published: 1 January 2018

Abstract: There is an increasing demand for cold-adapted enzymes in a wide range of industrial branches. Nevertheless, structural information about them is still scarce. The knowledge of crystal structures is important to understand their mode of action and to design genetically engineered enzymes with enhanced activity. The most difficult task and the limiting step in structural studies of cold-adapted enzymes is their crystallization, which should provide well-diffracting monocrystals. Herein, we present a combination of well-established crystallization methods with new protocols based on crystal seeding that allowed us to obtain well-diffracting crystals of two cold-adapted β-D-galactosidases (βDGs) from *Paracoccus* sp. 32d (*Par*βDG) and from *Arthrobacter* sp. 32cB (*Arth*βDG). Structural studies of both βDGs are important for designing efficient and inexpensive enzymatic tools for lactose removal and synthesis of galacto-oligosaccharides (GOS) and hetero-oligosaccharides (HOS), food additives proved to have a beneficial effect on the human immune system and intestinal flora. We also present the first crystal structure of *Arth*βDG (PDB ID: 6ETZ) determined at 1.9 Å resolution, and compare it to the *Par*βDG structure (PDB ID: 5EUV). In contrast to tetrameric *lacZ* βDG and hexameric βDG from *Arthrobacter* C2-2, both of these βDGs are dimers, unusual for the GH2 family. Additionally, we discuss the various crystallization seeding protocols, which allowed us to obtain *Par*βDG and *Arth*βDG monocrystals suitable for diffraction experiments.

Keywords: β-D-galactosidase; cold-adapted; lactose removal; microseeding; protein crystallization; crystal structure

1. Introduction

β-D-Galactosidases (EC 3.2.1.23) are widely used in the food industry as they catalyze the hydrolysis of terminal non-reducing β-D-galactose residue in β-D-galactosides. They are especially relevant in the dairy industry due to their ability to catalyze the hydrolysis of lactose, a natural substrate. Enzymatically hydrolyzed lactose, especially in milk, whey, or whey derivatives, is broadly used due to its higher sweetness, which ameliorates product taste, and to application in specialized food production, for people with lactose malabsorption [1–3]. Administration of products with depleted levels of lactose and other digestible oligosaccharides, disaccharides, monosaccharides, and polyols instead of common food is beneficial in the prevention of irritable bowel syndrome

(IBS) [4–9]. Cold-active β-D-galactosidases (βDGs) have become a focus of attention because of their ability to eliminate lactose from refrigerated milk, convert lactose to glucose and galactose (decreasing its hygroscopicity), and eliminate lactose from dairy industry pollutants associated with environmental problems. Moreover, in contrast to commercially available mesophilic β-D-galactosidase from *Kluyveromyces lactis*, the cold-active enzyme could make it possible to reduce the risk of mesophilic contamination and save energy during the industrial process connected with lactose hydrolysis [10–12].

In addition to hydrolytic activity, some β-D-galactosidases exhibit also a secondary transglycosylation activity, therefore they can be used for the synthesis of oligosaccharides (e.g., GOS and HOS) that are desirable functional food additives [13]. Such an activity is exhibited when there is a high concentration of a substrate and the galactose unit may be transferred onto the substrate, e.g., lactose. The oligosaccharides are built form D-galactose, D-glucose, N-acetylglucosamine, L-fucose, and sialic acid residues linked via O-glycosidic bonds. A vast majority of them carry lactose at their reducing end [14]. GOS are polymers of 2–10 D-galactose units, which are virtually not degraded by human digestive enzymes. Since they reach the colon practically intact and promote the growth of beneficial bacteria (*Bifidobacteria* and *Lactobacilli*), they are classified as prebiotics [15–18]. The importance of GOS as additive to infant formula-milk has been widely discussed as it has been proven not only to promote intestine colonization by beneficial bacteria but also to prevent bacterial adhesion in early stages of infection [14,16,19–24]. Moreover, some oligosaccharides are a rich source of sialic acid (essential for brain development) [25]. GOS and HOS are also valued additives to adult food, as recent research shows that they may increase mineral absorption [26–28], increase the rate of flu recovery, reduce stress-induced gastrointestinal disfunctions [29], as well as prevent cancer formation, benefit lipid metabolism, prevent hepatic encephalopathy, glycemia/insulinemia, and immunomodulation [30,31].

A typical oligomerization state of βDGs from GH2 is tetrameric [11,32] or hexameric [33]. However, large GH2 βDGs were reported to be active as functional dimers, based on biochemical investigations [34,35]. The crystal structure of the first dimeric GH2 βDG was recently published by us [36]; however, that enzyme is much smaller than typical GH2 βDGs (a monomer of only 70 kDa) and exhibits a different shape and orientation of domain 5, called wind-up domain.

Despite extensive efforts and application of different methods for the crystallization of cold adapted proteins, the process is still challenging, as in the Protein Data Bank (PDB) only around 40 crystal structures of cold-adapted enzymes are available, which is a small percentage of 132,000 total structures deposited in the PDB. Whereas the structures of multiple mesophilic βDGs are known, only two structures of cold-adapted βDGs have been previously deposited in the PDB [33,36] and the obtained results show that the investigated enzyme differs in tertiary and quaternary structure from the previously described ones. Here we describe the crystallization methods used to ameliorate and control crystallization of cold adapted *Parβ*DG and *Arth*βDG, as well as crystal structure determination of *Arth*βDG, the second cold-active βDG from the GH2 family identified as dimeric up to a year ago.

2. Materials and Methods

2.1. ArthβDG Production

The heterologous expression of the recombinant β-D-galactosidase from *Arthrobacter* sp. 32cB was performed in the *E. coli* LMG 194 cells transformed with pBAD-Bgal 32cB plasmid under the control of P_{BAD} promoter (Table 1). For the production of *Arth*βDG, the *E. coli* cells were grown at 30 °C in Luria-Bertani (LB) medium supplemented with 100 μg/mL ampicillin, until an OD_{600} of 0.5 was reached. Overexpression was induced by addition of 20% L-arabinose solution to the final concentration of 0.02%. The culture was further cultivated for 15 h to OD_{600} of 3.8 ± 0.2 and harvested by centrifugation (6000 × *g*, 15 min, 4 °C) [37].

Table 1. *Arthrobacter* sp. 32cB production information.

Source Organism	*Arthrobacter* sp. 32cB
DNA source	Genomic DNA
Forward primer	F232cBNco (*Nco*I restriction site underlined) TCTACCATGGCTGTCGAAACACCGTCCGCGCTGGCGGAT
Reverse primer	R32cBHind (*Hin*dIII restriction site underlined) TGACAAGCTTCAGCTGCGCACCTTCAGGGTCAGTATGAAG
Cloning vector	pBAD/Myc-His A (Invitrogen, Carlsbad, CA, USA)
Expression vector	pBAD-Bgal 32cB
Expression host	*E. coli* LMG194 (Invitrogen, Carlsbad, CA, USA)

The extraction of intracellular protein was carried out by two separate methods. Method 1: The cells were resuspended in buffer A containing: 20 mM K_2HPO_4/KH_2PO_4 (pH 6.0), 50 mM KCl and the cell suspension was disrupted by sonication on an ice bath using 20 repetitions of 15 s impulses with 60 s pauses to avoid sample overheating. The lysate was clarified by centrifugation at 4 °C for 30 min at 9000 × *g* [37]. Method 2: The cell pellet was ground into a fine powder in a mortar and pestle under liquid nitrogen, with addition of silicone beads. The powder was resuspended in buffer A, and the sample was clarified by centrifugation at 4 °C for 30 min at 9 000 × *g*.

2.2. Purification of ArthβDG

*Arth*βDG was purified by two ion-exchange chromatography steps (weak anion exchanger and strong anion exchanger), followed by a size-exclusion chromatography step. The cell-free supernatant was loaded onto a DEAE (BioRad, Hercules, CA, USA) column equilibrated with buffer A (20 mM K_2HPO_4/KH_2PO_4 (pH 6.0), 50 mM KCl). The recombinant *Arth*βDG was eluted using a linear gradient of potassium chloride (20–1020 mM) in the same buffer. The fractions containing *Arth*βDG were determined and dialyzed against buffer A. In the second step, the protein sample was loaded onto HiPrep Q Sepharose 16/10 column (GE Healthcare, Little Chalfont, UK) equilibrated with buffer A and eluted with a linear gradient of potassium chloride (20–820 mM) in the same buffer. Fractions containing *Arth*βDG were once again determined and dialyzed against buffer C (20 mM K_2HPO_4/KH_2PO_4 (pH 7.5), 150 mM KCl). The concentrated sample was injected onto a Superdex 200 column (GE Healthcare, Little Chalfont, UK), previously equilibrated with buffer C.

The fractions containing *Arth*βDG were identified by SDS-PAGE electrophoresis run at 10% SDS-polyacrylamide gel and by enzymatic activity assay, in parallel. The determination of fractions containing active βDG may be readily validated by enzymatic activity assay: 10% *ortho*-nitrophenyl-β-D-galactopyranoside (ONPG) was added to the sample (1:4 ratio). Sample color change into intense yellow was observed for samples containing βDG. The sample of buffer coming from the chromatography column was changed into 0.05 M HEPES pH 7.0 and the samples were concentrated using 50 kDa cutoff membrane Vivaspin filters (Sartorius, Göttingen, Germany).

2.3. ParβDG and ArthβDG Crystallization

All crystallizations were performed in 24-well plates (Hampton Research, Aliso Viejo, CA, USA) using hanging drop vapor-diffusion method at 18 °C. The 1 µL drop of protein was placed on siliconized glass cover slide, covered with an equal volume of reservoir solution and left to equilibrate against 500 µL of crystallization buffer.

First crystallization conditions for *Par*βDG were found using PEG/Ion Screen™ HR2-126 and Index Screen™ HR2-144 (Hampton Research, Aliso Viejo, CA, USA). Initial optimization of crystallization conditions was performed using varying concentrations of precipitants (PEG MME 2K and ammonium acetate), as well as various pHs. To further improve the crystal morphology, various additives were tried from commercially available Additive Screen (Hampton Research, Aliso Viejo, CA, USA).

Initial crystal screenings used for *Arth*βDG crystallization were: Index Screen™ HR2-144, PEG/Ion Screen™ HR2-126, PEG/Ion2 Screen™ HR2-089 (Hampton Research, Aliso Viejo, CA, USA), and Morpheus® HT-96 (Molecular Dimensions, Suffolk, UK).

2.3.1. Streak Seeding

The seed stock was prepared using the previously obtained hair-type crystals. The crystals were transferred to a tube containing a small volume of reservoir solution (around 20 µL) and the crystals were crushed with a pipette tip. Subsequently, the concentrated seed stock was diluted several times by addition of a larger volume of reservoir solution (~100 µL). The crystallization plate was set up using the previously optimized crystallization conditions. The protein solution was slightly diluted (to 13 mg/mL), premixed with dichloromethane at the final concentration of 0.025% (v/v) and the drops were set in a 1:1 ratio. The cover slides with the drops were sealed and the plate was left for a short pre-equilibration time intact. The hair was run through the seed stock and then through the freshly set drops.

2.3.2. Seed Stock Preparation

The obtained *Arth*βDG crystals were crushed within a crystallization drop with a CrystalProbe (Hampton Research, Aliso Vieja, CA, USA). Next, they were carefully transferred into 50 µL of cool reservoir solution and the solution was vortexed with addition of SeedBead (Hampton Research, Aliso Vieja, CA, USA), kept cool all the time. A series of dilutions of such prepared seed stock was performed and systematic (10×) dilution was used for the rMMS crystallization experiment.

2.3.3. Random Microseed Matrix Screening Crystallization

The procedure rMMS was applied for screening co-crystallization conditions of *Arth*βDG complexes with ligands such as lactose and IPTG. The screening was performed at 18 °C using the sitting drop vapor diffusion technique with an automated sample handling robotic system Oryx4 (Douglas Instruments Ltd., Hungerford, UK) [38]. The drop was composed of: 0.20 µL of protein, 0.07 µL of seed solution and 0.13 µL of reservoir, and placed over 50 µL of reservoir solution. The screens such as PEG/Ion Screen™ HR2-126, PEG/Ion2 Screen™ HR2-098 (Hampton Research, Aliso Vieja, CA, USA), and Morpheus® HT-96 (Molecular Dimensions, Suffolk, UK) were tested for alternative co-crystallization conditions for complexes of *Arth*βDG.

2.4. Data Collection and Processing

Initial X-ray diffraction measurement of the crystals was performed at our home source SuperNova (Rigaku Oxford Diffraction, Tokyo, Japan). High-resolution data were collected using a synchrotron source on beamline BL14.2 at BESSY, Berlin, Germany. For some crystals, 1.8 M sodium malonate, 60% Tacsimate™ (both with appropriate pH) or 50% glycerol solution was used as cryoprotectant during the data collection. Generally cryoprotectants containing only salts of carboxylic acids worked better than those containing glycerol [39]. The diffraction data were processed with XDSapp [40]. The details for the data collection and processing of *Arth*βDG are presented in Table 2.

Table 2. The diffraction data collection and processing statistics for *Arth*βDG crystal PDB ID: 6ETZ.

Diffraction Source	BL 14.2 BESSY, Berlin, Germany
Wavelength (Å)	0.918400
Temperature (K)	100 K
Detector	PILATUS 3S 2M
Crystal-detector distance (mm)	344.48
Rotation range per image (°)	0.1

Table 2. *Cont.*

Diffraction Source	BL 14.2 BESSY, Berlin, Germany
Total rotation range (°)	180
Exposure time per image (s)	0.3
Space group	$P3_121$
a, *b*, *c* (Å)	137.78, 137.78, 127.20
α, β, γ (°)	90, 90, 120
Mosaicity (°)	0.077
Resolution range (Å)	46.7–1.8 (1.9–1.8)
Total No. of reflections	1305805
No. of unique reflections	129004
Completeness (%)	99.5 (97.9)
Redundancy	9.98 (9.59)
I/σ(I)	14.46 (1.5)
R_{meas} (%)	11.3 (136.1)
Overall *B* factor from Wilson plot (Å^2)	25.6

Values for the outer shell are given in parentheses.

2.5. Structure Solution and Refinement

The Matthews value calculation showed that a monomer of protein is present in the asymmetric unit. The structure of *Arth*βDG was solved by molecular replacement using a monomer of the closest homologue structure (PDB ID: 1YQ2): βDG from *Arthrobacter* C2-2 [33] with the program *PHASER* [41]. The model after rebuilding in *COOT* [42], which was possible due to the significant 2*Fo-Fc* electron density map for the missing fragments, after first cycle of refinement in *REFMAC5* [43] gave R_{work} and R_{free} values of 19.6% and 23.1%, respectively. That model was further refined in *REFMAC5* using maximum-likelihood targets, including TLS parameters [44] defined for each domain, yielding the final R_{work} and R_{free} of 16.1% and 19.8%, respectively (Table 3).

Table 3. *Arth*βDG crystal structure solution and refinement parameters.

	PDB ID: 6ETZ
Resolution range (Å)	46.73–1.80 (1.84–1.80)
Completeness (%)	99.5
No. of reflections, working set	126888 (8872)
No. of reflections, test set	2100 (146)
Final R_{cryst}	0.161 (0.303)
Final R_{free}	0.198 (0.314)
Cruickshank DPI	0.0913
No. of non-H atoms:	
Protein	7727
Ion	1
Ligand	23
Water	1183
Total	8934
R.m.s. deviations	
Bonds (Å)	0.019
Angles (°)	1.874
Ramachandran plot:	
Most favored (%)	98
Allowed (%)	2

Values for the outer shell are given in parentheses.

3. Results and Discussion

3.1. Crystallization of Cold-Adapted βDGs

3.1.1. Crystallization of Cold-Adapted *Par*βDG

The crystal structure of *Par*βDG has been already reported in our previous article [36] that focused on its structural analysis (PDB ID: 5EUV). The crystallization process was not discussed there in detail. Therefore, here we describe all steps that were necessary to obtain monocrystals with good diffraction properties.

Since *Par*βDG purification has already been described [36], it will be mentioned only briefly. The protein was expressed in *E. coli* and purified using a two-step protocol employing ion exchange chromatography: the first step was carried out using Fractogel EMD DEAE column (Merck, Darmstadt, Germany) and was followed by a protein separation on a Resource Q column (Merck, Darmstadt, Germany). The active fractions of *Par*βDG were dialyzed against a buffer composed of 0.02 M sodium phosphate, pH 7.3. The protein was concentrated to 15 mg/mL.

The standard crystallization screening performed for *Par*βDG gave clustered hair-like crystals in 24% PEG MME 2K, 0.1 M ammonium acetate, 0.1 M Bis-Tris, pH 6.0 (Figure 1a). After an optimization of the crystallization conditions, a decrease of pH to 5.5 improved slightly the morphology of the *Par*βDG crystals (Figure 1b). Several crystals present in the cluster became thin needles. However, it was still difficult to separate them from the cluster.

Various additives, 96 in total, were tested (Additive Screen, Hampton Research, Aliso Vieja, CA, USA), and the best results were obtained using the previously optimized crystallization conditions and dichloromethane at a final concentration of 0.025% (v/v) as an additive premixed with protein. Some of the crystals still formed hair-type clusters; however, a number of separate needles could be observed in the drops (Figure 1c).

The single needles were obtained by a combination of crystallization with the additive and streak seeding, where the hair was run through a seed stock and then through the freshly set drops. After the second round of seeding, we obtained crystals that grew as separate needles (Figure 1d). The final protein concentration used for setting the drops was 11 mg/mL. The decrease of the protein concentration and introduction of the seeds to the drops enabled significantly improved crystal growth.

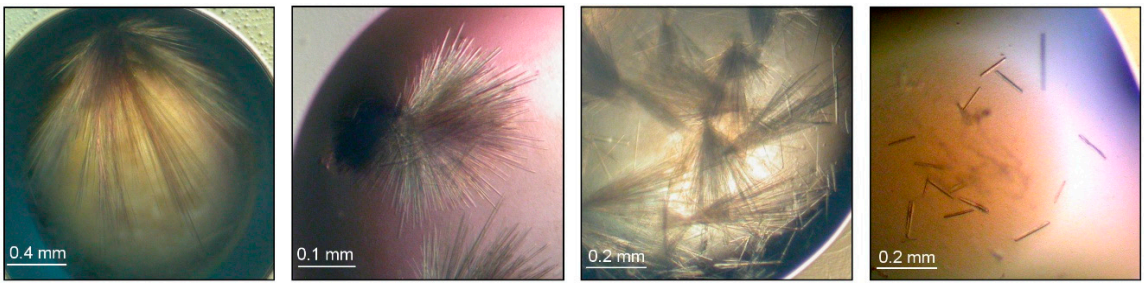

Figure 1. *Par*βDG crystals: (**a**) initial screening (pH 6); (**b**) initial optimization (pH 5.5); (**c**) the optimization with Additive Screen; (**d**) crystals obtained with streak seeding.

3.1.2. Crystallization of Cold-Adapted *Arth*βDG

*Arth*βDG was produced in *E. coli* as a soluble, intracellular recombinant protein. For its extraction from the cells two methods were used in parallel. Although extraction with mortar and pestle under liquid nitrogen is a time and energy consuming process, it proved to be more beneficial for subsequent protein crystallization than classical sonication. Not only a higher yield of purification was obtained for this extraction method, but the growth of native crystals was more rapid. The first crystals were observed after 3 days, whereas for the protein extracted using sonication the first crystals occurred

after 5 days (under corresponding crystallization conditions). Subsequent to extraction, *Arth*βDG was purified using two steps of ion-exchange and the third step was size-exclusion chromatography. The whole purification procedure was conducted at 4 °C, as the protein samples purified at higher temperature (e.g., 18 °C) produced no crystals even under previously determined crystallization conditions. The cold-adapted enzymes exhibit higher propensity towards thermal denaturation [45], the resulting denaturation or unfolding negatively affects subsequent crystallization. The eluted fractions were tested using an enzymatic assay [46], and the ones exhibiting hydrolytic activity versus ONPG were further analyzed by SDS-PAGE electrophoresis. The recombinant *Arth*βDG migrated on an SDS-polyacrylamide gel with a molecular weight of ~110 kDa, which was in agreement with the calculated molecular mass of its monomer based on a cloned construct. The observation of a sharp peak of protein during the last step of purification and the presence of a sole band on an electrophoretic gel proved that the sample was highly purified (Figure 2).

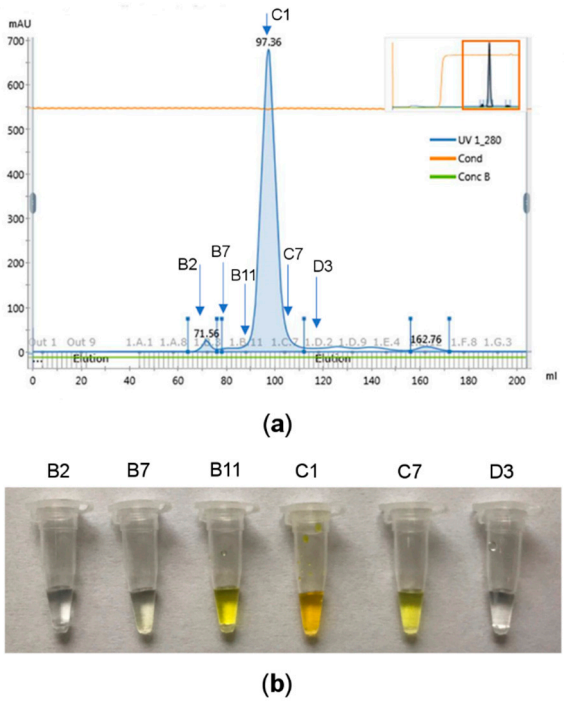

Figure 2. *Arth*βDG purification results: (**a**) protein peak purified and concentrated by size-exclusion chromatography, the fractions indicated with arrows were used for enzymatic assay; (**b**) results of the enzymatic assay. The selected protein samples were added to 10% *ortho*-Nitrophenyl-β-D-galactopyranoside (ONPG) solution. The yellow color is produced by ortho-nitrophenol obtained by enzymatic hydrolysis of ONPG, thus indicating fractions with βDG activity (B11, C1, C7), the other tested fractions exhibited no βDG activity (B2, B7, D3); all the fractions from range B11–C7 were combined and used for crystallization experiments.

The initial crystallization screening was performed using the same range of *Arth*βDG concentration (6–12 mg/mL) as we used previously to obtain crystals of cold-adapted aminotransferase from *Psychrobacter* sp. B6 (*Psy*ArAT) [46]. No crystals were observed for a sample concentration below 10 mg/mL. For the protein concentration exceeding 10 mg/mL, a few conditions yielded small crystals, whose size did not exceed 0.02 × 0.02 × 0.02 mm, or microcrystalline precipitate. However, none of them were directly suitable for diffraction experiments. Thus, for crystallization optimization, a sample concentration of 10 mg/mL was used. The optimized crystallization conditions included precipitants such as: sodium malonate, sodium phosphate, potassium phosphate, ammonium sulfate, pentaerythriol etoxylate, L-proline, sodium citrate, PEG 3350, Jeffamine-2001, and Tacsimate™ (Hampton Research, Aliso Vieja, CA, USA). As a result, we obtained larger (up to 0.3 × 0.2 × 0.2 mm)

*Arth*βDG crystals in a tetragonal or bipyramidal form in conditions containing 1.4 M sodium malonate, 1.5% Jeffamine, and 0.1 M HEPES pH 7.0 (Figure 3d), and smaller (up to 0.2 × 0.2 × 0.15 mm) crystals of the same morphology from 35% Tacsimate™ pH 8.0 (Figure 3c). The optimization of precipitating solutions containing PEG 3350 and inorganic salts yielded no monocrystals. No better quality crystals of *Arth*βDG were obtained for crystallization held at 4 °C, regardless of the concept that lowering the experiment temperature, thus thermal energy, should aid crystallization of highly flexible proteins. It might have been caused by its relatively high, as for cold-adapted protein, thermal optimum of 28 °C [37].

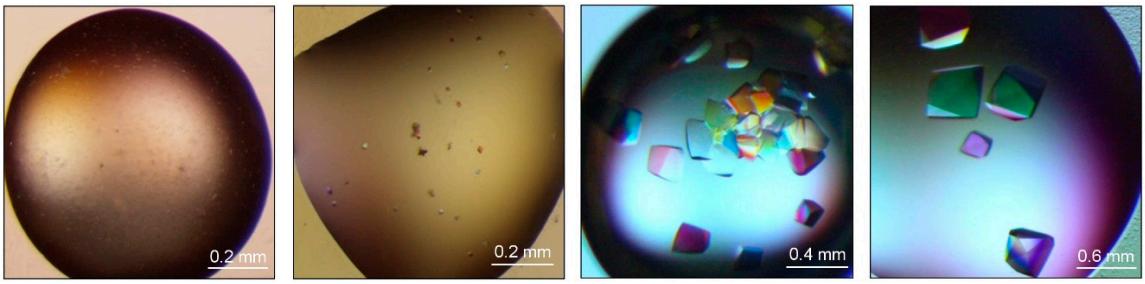

Figure 3. *Arth*βDG crystals. The best results of the initial screening: (**a**) crystallization conditions containing 1.1 M sodium malonate pH 7.0, 0.1 M HEPES pH 7.0, 0.5% Jeffamine® ED-2001 pH 7.0; (**b**) 30% Tacsimate™ pH 7.0; results of the optimization: (**c**) crystallization conditions containing 35% Tacsimate pH 8.0; (**d**) 1.4 M sodium malonate, 0.1 M HEPES pH 7.0, 1.5% Jeffamine® ED-2001 pH 7.0.

The diffraction experiment performed on initial larger crystals (Figure 3b) using a home source SuperNova diffractometer proved that they were of protein; however, their diffraction, due to the small size, was very poor (~8 Å). Further optimization of crystallization conditions and subsequent measurements utilizing synchrotron radiation allowed us to collect complete diffraction datasets with a resolution up to 2.2 Å for large crystals (Figure 3d) (Figure 4a) and up to 1.8 Å for a little smaller (but still big) crystals (Figure 3c) (Figure 4b). Even though the sizes of crystals from 35% Tacsimate™ pH 8.0 were smaller, the resulting diffraction data had higher resolution.

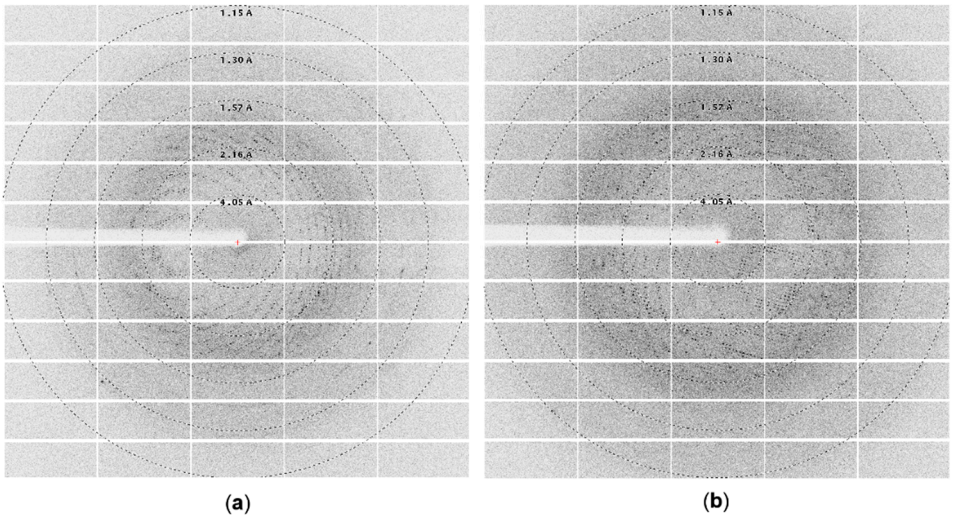

Figure 4. Diffraction images collected on BL 14.2 line BESSY synchrotron : (**a**) using *Arth*βDG crystal crystallized in the presence of 1.4 M sodium malonate, 1.5% Jeffamine, and 0.1 M HEPES pH 7.0; (**b**) using *Arth*βDG crystal crystallized in the presence of 35% Tacsimate™ pH 8.0.

Since the crystallization conditions included a high concentration of organic acids that might have been preventing ligand binding, the search for alternative crystallization conditions for complexes of *Arth*βDG with isopropyl β-D-1-thiogalactopyranoside (IPTG) and lactose was performed using the random Microseed Matrix Screening (rMMS) procedure. The introduction of seed stock to crystallization drops allowed us to determine multiple crystallization conditions, containing a minimal concentration of Tacsimate^{TM} (introduced with seeds). It is of note that the hits were partially different depending on the used ligand (Figure 5).

Another issue with *Arth*βDG crystals obtained using the classical hanging drop vapor diffusion method was that crystals, which grew in the same drop possessing the same morphology and of a similar size, were randomly diffracting well (~2 Å) or very poorly (~10 Å). To ensure the required quantity of well diffracting crystals, the seeding of the known crystallization conditions was performed. Different seed stock dilutions, 10×, 100×, 1000×, and different protein concentrations, 6 mg/mL, 8 mg/mL, and 10 mg/mL were examined. The use of 8 mg/mL protein concentration and 1000× diluted seed stock yielded formation of ~10 diffracting crystals per drop with average dimensions of 0.25 × 0.2 × 0.2 mm. The adaptation of the seeding procedure for setting up crystallization manually was performed: 6% v/v of cool seed stock was added to the cooled protein solution directly, right before drop setting. The sample was kept on ice for the time of operations. The crystallization was then set up using the standard hanging drop procedure. Introduction of altered crystallization seeding and lowering the protein concentration to 8 mg/mL proved to reproducibly yield diffracting quality crystals. The number of crystals in a drop could be controlled by the use of different dilutions of readily available, pre-prepared and frozen seed stock.

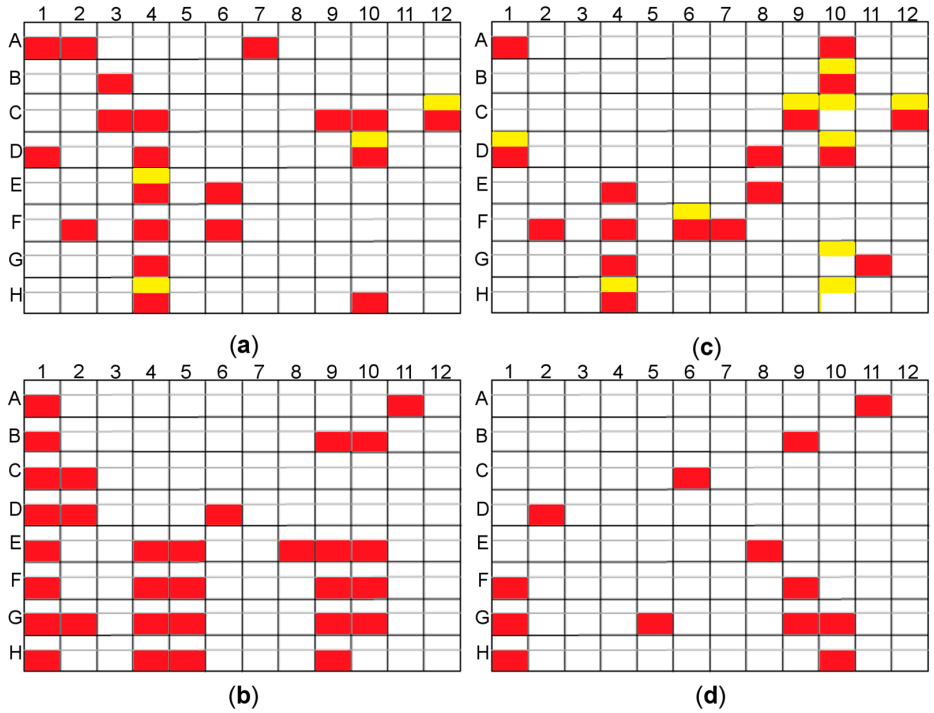

Figure 5. The results of the rMMS experiments for two screen sets depending on the ligand added; yellow–crystals obtained with no seeding (control), red–crystals obtained by seeding; (**a**) PEG/Ion and PEG/Ion2 screen *Arth*βDG co-crystallized with lactose; (**b**) Morpheus and Morpheus II screen *Arth*βDG co-crystallized with isopropyl β-D-1-thiogalactopyranoside (IPTG); (**c**) PEG/Ion and PEG/Ion2 screen *Arth*βDG co-crystallized with IPTG; (**d**) Morpheus and Morpheus II screen *Arth*βDG co-crystallized with lactose. Some of the obtained crystals were big enough for diffraction experiment, e.g., plate (a) A7, plate (b) D8, however most of the obtained crystal hits needed further optimization. Use of microseeding enabled the picking up of a considerable amount of new hits.

3.2. Structure of ArthβDG

3.2.1. Overall Fold

The crystal structure of *Arth*βDG (PDB ID: 6ETZ) revealed that the protein consists of five domains: (Domain 1 (Ser24-Pro224), Domain 2 (Asp225-Gly310), Domain 3 (Ser311-Pro606), Domain 4 (Leu607-Val716), and Domain 5 (Pro717-Ser1010)), with the catalytic one being TIM-barrel, which is typical for glycoside hydrolases. The other four domains, each with an immunoglobulin-like fold, surround Domain 3 and form the outer surface of the functional dimer. Domain 1, Domain 2, and Domain 4 are jelly-roll type barrels. Domain 5 (Pro717-Ser1010) is a large β-sandwich domain (Figure 6). The long linker between Domain 4 and Domain 5, comprising a high number of proline residues, provides some rigidity to this highly solvent exposed fragment. Regardless of low sequence similarity (35%) (Figure S1), *Arth*βDG monomer has an overall fold similar to the characteristics for this group of enzymes *E. coli* lacZ βDG. The intriguing questions, why nature produced such a big multi-domain enzyme to perform a relatively simple reaction, and what is the function of the surrounding domains, still remain open.

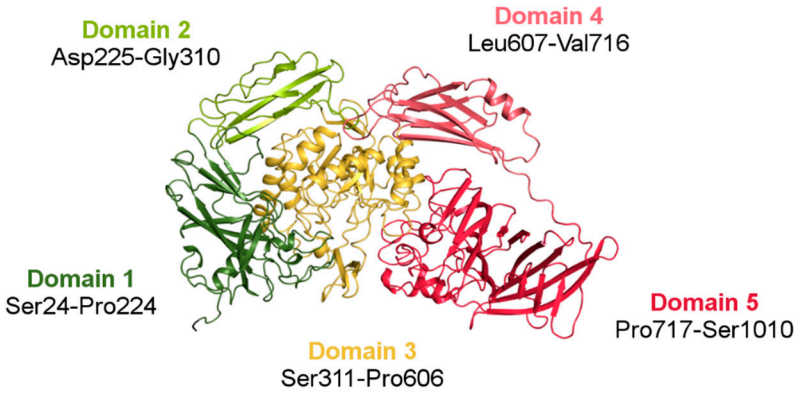

Figure 6. A monomer of *Arth*βDG (PDB ID: 6ETZ) colored by domain. The central catalytic Domain 3 (gold) is typical for the GH2 family TIM-barrel fold. The Domains 1 (dark green) and 5 (red) are responsible for intramolecular contacts forming a biologically active dimer.

3.2.2. Architecture of the Functional Dimer

*Arth*βDG acts as a head-to-tail dimer, with two independent active sites. Even though only a monomer is present in the asymmetric unit of *Arth*βDG crystal, the functional dimer is mapped by the symmetry operations. The *Arth*βDG dimer interface is made by extensive contacts between Domain 1 interacting with Domain 5 of an adjacent monomer (Figure 7a). *Par*βDG acts also as a functional dimer, which is present in the asymmetric unit of the crystal [36]. The active site of these enzymes is created by residues belonging to both monomers of the dimer. The presence of the dimers in solution was confirmed by gel filtration chromatography (Figure S2), for both enzymes [36]. The *Par*βDG dimer is more elongated and its interface is made by extensive contacts between Domain 3 interacting with Domain 4 of an adjacent monomer and Domains 5 from both monomers (Figure 7b).

The architecture of the functional dimer of *Arth*βDG differs significantly from the functional dimer of *Par*βDG (Figure 7). The buried area of the *Par*βDG dimer is 7180 Å^2, while of the substantially larger *Arth*βDG, 6150 Å^2, the assemblies analysis was performed using a PISA server (Table 4) [47].

Crystal structures of these two enzymes indicate that the biological assembly arrangement is an important factor as to why *Par*βDG exhibits low transglycosylation activity. The cramped vicinity of *Par*βDG active site, and its deep location limits possible galactosyl group acceptors to primarly water molecules. By contrast, the more spacious and easily substrate-accessible active site of *Arth*βDG allows molecules such as galactose, fructose, or salicin, to be acceptors for transfer of the galactosyl group (Figure 8b).

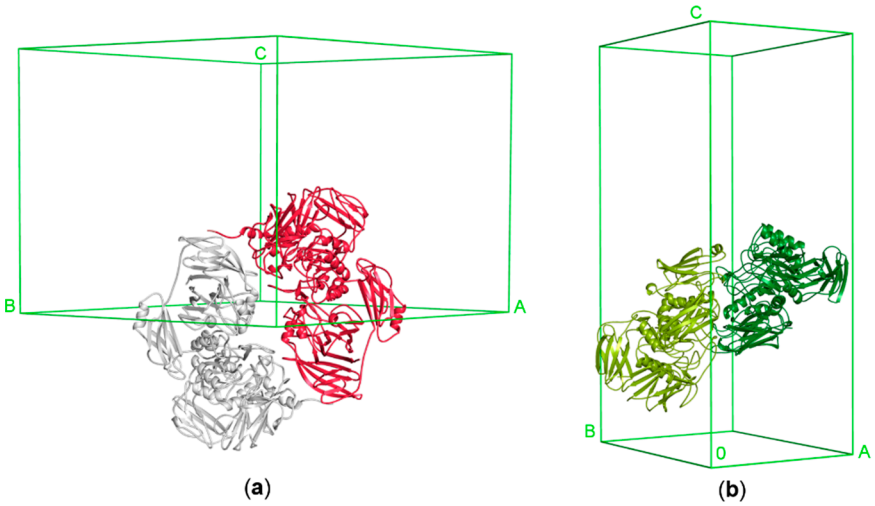

Figure 7. The functional dimers of *Arth*βDG and *Par*βDG in unit cells: (**a**) *Arth*βDG (PDB ID: 6ETZ); (**b**) *Par*βDG (PDB ID: 5EUV).

Table 4. PISA assembly analysis of *Par*βDG and *Arth*βDG.

Protein	Composition	Surface Area [Å^2]	Buried Area [Å^2]	ΔG^{int} [kcal/mol]	ΔG^{diss} [kcal/mol]
*Par*βDG	dimer	48 760	7 180	−17.5	24.8
*Arth*βDG	dimer	68 700	6 150	−28.9	6.3

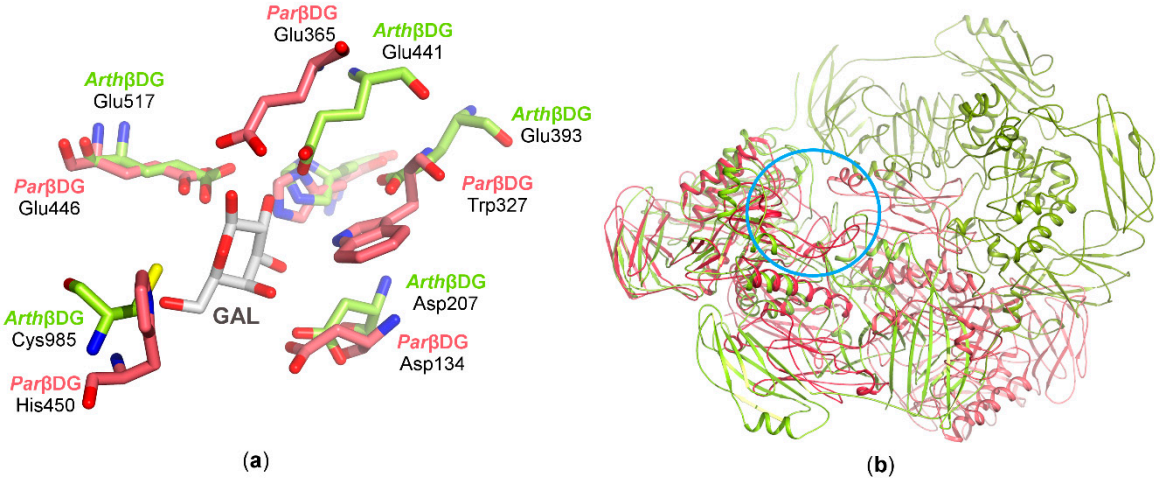

Figure 8. The superposition of *Arth*βDG and *Par*βDG in complex with galactose: (**a**) residues in active sites involved in galactose binding; (**b**) the superposition of biologically active dimers with superposed active sites (marked with a blue circle) of monomers A (*Par*βDG presented in shades of red and *Arth*βDG in shades of green).

3.2.3. Catalytic Center

In both enzymes the catalytic domain is a highly conserved TIM-barrel, which contains eight parallel β-strands and seven α-helices. The catalytic residues were determined to be Glu441, Glu517 in *Arth*βDG and Glu365, Glu446 in *Par*βDG. A superposition of the active sites of *Arth*βDG with the other two cold-adapted βDGs, as well as their superpositions with homologous mesophilic GH2 βDG, revealed that the catalytic center is highly conserved in this group of enzymes.

A superposition of *Arth*βDG with *Par*βDG shows extensive similarity in the region of the catalytic amino acids; however, other parts of the catalytic center exhibit large differences (Figure 8a). Superimposed catalytic centers of both βDGs show that, besides identical catalytic amino acid residues stabilizing galactose binding, His302/His368 and Asp134/Asp207 are also conserved. However, differences in some residues, His450/Cys985 and Trp327/Glu393, result in alteration of active sites shape, volume, and character. The overlay of the biological dimers indicates how the differences in their assemblies influence the substrate selectivity.

The presence of the non-proline *cis*-peptide bonds in the close vicinity of active sites is a very intriguing observation, as such bonds are extremely rare. Two of them are crucial for the creation of an active site, as they constitute its bottom, and therefore regulate its volume. A comparison with other GH2 βDGs revealed that all three observed non-proline *cis*-peptides are present in the same places in this family of enzymes. Moreover, they are common for all glycoside hydrolases that catalyze the reaction with the retaining configuration on anomeric carbon of hydrolyzed β-glycoside.

4. Conclusions

Generally, nucleation is a critical stage in the crystallization of proteins, and for those possessing conformationally labile fragments, as e.g., cold adapted enzymes, it is a bottleneck of crystal structure determination, and it is necessary to implement factors lowering the nucleation barrier.

By implementation of different seeding techniques, such as streak seeding, in situ random microseeding, and streak microseeding, crystallization of two cold-adapted βDGs was successful. Further, the microseeding allowed us to obtain diffraction quality crystals in a routine manner, which significantly simplified further structural studies of these proteins and reduced uncertainties connected with the crystallization stage. Additionally, the used techniques of microseeding allowed growing crystals after nucleation (coming from seeds) without achieving oversaturation.

In the case of cold-adapted proteins, which are more prone to thermal denaturation then mesophilic enzymes, the temperature factor must be taken into account at all stages of protein preparation. In the case of *Arth*βDG, we were able to obtain more protein sample from the same volume of biomass when we used mortar and pestle under liquid nitrogen instead of sonication. The sonication produces a large amount of heat, even though extensive sample cooling was introduced into the protocol, the cold-adapted *Arth*βDG was too sensitive for this method. The next step, chromatographic purification, was even more susceptible to temperature elevation due to its long overall time. We were able to obtain well crystallizing protein samples only when the whole purification procedure was conducted at 4 °C.

The crystal structure of *Arth*βDG, as well as establishing purification and crystallization protocols, gives a good starting point for further crystallographic analysis of this enzyme aiming at its activity engineering [48]. The comparison of its catalytic center, with other βDGs indicates putative residues involved in the transglycosylation reaction.

Supplementary Materials: The following are available online at www.mdpi.com/2073-4352/8/1/13/s1. Figure S1: The sequence alignment of *Arth*βDG and *Par*βDG performed using EMBOSS Needle Pairwise Sequence Alignment. The sequence similarity is 35%, and identity only 17.6% with 47.3% gaps. Catalytic amino acids marked with red boxes; Figure S2: Biochemical oligomerization assays of *Arth*βDG. (a) SDS-PAGE analysis stained with Coomasie Brillant Blue G; lane 1 protein molecular-weight markers (Thermo Fisher Scientific), lane 2 *Arth*βDG; (b) V_e/V_0 versus log MW calibration curve for separation of proteins on a Superdex 200 10/200 GL column with *Arth*βDG marked red (V_e, elution volume; V_0, void volume); (c) chromatographic separation of the fraction containing active *Arth*βDG by gel filtration on a Superdex 200 10/300 GL column.

Acknowledgments: This research was supported by grant 2016/21/B/ST5/00555 (A.B.) from the National Science Centre, Poland. We thank Patrick Shaw Stewart for providing a possibility to test Oryx4 (Douglas Instruments Ltd., East Garston, UK) using our samples. We thank the HZB BESSY Berlin, Germany for providing access to BL 14.2 beamline and MX staff for providing support on beamline. We are grateful to A. Wlodawer, NCI for help with editing the manuscript.

Author Contributions: Maria Rutkiewicz-Krotewicz and Agnieszka J. Pietrzyk-Brzezinska performed crystallization of βDGs; Maria Rutkiewicz-Krotewicz and Anna Bujacz performed synchrotron diffraction data collection, processing, structure solving and carried out structural analysis. Maria Rutkiewicz-Krotewicz purified enzyme, refined the structure and mostly wrote the paper to which Anna Bujacz and Agnieszka J. Pietrzyk-Brzezinska also contributed. Marta Wanarska and Hubert Cieslinski performed enzymes expression in *E. coli* and determined the purification protocol. Anna Bujacz coordinated the project.

Conflicts of Interest: The authors declare no conflict of interest.

References

1. Pritzwald-Stegmann, B.F. Lactose and some of its derivatives. *Int. J. Dairy Technol.* **1986**, *39*, 91–97. [CrossRef]
2. Khan, M.; Husain, Q.; Bushra, R. Immobilization of β-galactosidase on surface modified cobalt/multiwalled carbon nanotube nanocomposite improves enzyme stability and resistance to inhibitor. *Int. J. Biol. Macromol.* **2017**, *105*, 693–701. [CrossRef] [PubMed]
3. Traffano-Schiffo, M.V.; Castro-Giraldez, M.; Fito, P.J.; Santagapita, P.R. Encapsulation of lactase in Ca(II)-alginate beads: Effect of stabilizers and drying methods. *Food Res. Int.* **2017**, *1000*, 296–303. [CrossRef] [PubMed]
4. Borghini, R.; Donato, G.; Alvaro, D.; Picarelli, A. New insights in IBS-like disorders: Pandora's box has been opened; a review. *Gastroenterol. Hepatol. Bed Bench* **2017**, *10*, 79–89. [PubMed]
5. Rossi, M.; Aggio, R.; Staudacher, H.M.; Lomer, M.C.; Lindsay, J.O.; Irving, P.; Probert, C.; Whelan, K. Volatile organic compounds in feces associate with response to dietary intervention in patients with irritable bowel syndrome. *Clin. Gastroenterol. Hepatol.* **2017**, *S1542–S3565*, 31201–31216. [CrossRef] [PubMed]
6. Staudacher, H.M.; Lomer, M.C.E.; Farquharson, F.M.; Louis, P.; Fava, F.; Franciosi, E.; Scholz, M.; Tuohy, K.M.; Lindsay, J.O.; Irving, P.; et al. A diet low in fodmaps reduces symptoms in patients with irritable bowel syndrome and a probiotic restores *Bifidobacterium* species: A randomized controlled trial. *Gastroenterology* **2017**, *153*, 936–947. [CrossRef] [PubMed]
7. Cozma-Petrut, A.; Loghin, F.; Miere, D.; Dumitraşcu, D.L. Diet in irritable bowel syndrome: What to recommend, not what to forbid to patients! *World J. Gastroenterol.* **2017**, *23*, 3771–3783. [CrossRef] [PubMed]
8. Yuce, O.; Kalayci, A.G.; Comba, A.; Eren, E.; Caltepe, G. Lactose and fructose intolerance in Turkish children with chronic abdominal pain. *Indian Pediatr.* **2016**, *53*, 394–407. [CrossRef] [PubMed]
9. Pawłowska, K.; Umławska, W.; Iwańczak, B. Prevalence of lactose malabsorption and lactose intolerance in pediatric patients with selected gastrointestinal diseases. *Adv. Clin. Exp. Med.* **2015**, *24*, 863–871. [CrossRef] [PubMed]
10. Wierzbicka-Wos, A.; Cieslinski, H.; Wanarska, M.; Kozlowska-Tylingo, K.; Hildebrandt, P.; Kur, J. A novel cold-active β-D-galactosidase from the *Paracoccus* sp. 32d-gene cloning, purification and characterization. *Microb. Cell Fact.* **2011**, *10*, 108–119. [CrossRef] [PubMed]
11. Bialkowska, A.M.; Cieslinski, H.; Nowakowska, K.M.; Kur, J.; Turkiewicz, M. A new beta-galactosidase with a low temperature optimum isolated from the Antarctic *Arthrobacter* sp. 20B: Gene cloning, purification and characterization. *Arch. Microbiol.* **2009**, *191*, 825–835. [CrossRef] [PubMed]
12. Cavicchioli, R.; Charlto, T.; Ertan, H.; Mohd Omar, S.; Siddiqui, K.S.; Williams, T.J. Biotechnological uses of enzymes from psychrophiles. *Microb. Biotechnol.* **2011**, *4*, 449–460. [CrossRef] [PubMed]
13. Harju, M. Milk sugars and minerals as ingredients. *Int. J. Dairy Technol.* **2001**, *54*, 61–63. [CrossRef]
14. Kunz, C.; Rudloff, S. Biological functions of oligosaccharides in human milk. *Acta Paediatr.* **1993**, *82*, 903–912. [CrossRef] [PubMed]
15. Boehm, G.; Fanaro, S.; Jelinek, J.; Stahl, B.; Marini, A. Prebiotic concept for infant nutrition. *Acta Paediatr.* **2003**, *92*, 64–67. [CrossRef]
16. Chierici, R.; Fanaro, S.; Saccomandi, D.; Vigi, V. Advances in the modulation of the microbial ecology of the gut in early infancy. *Acta Paediatr.* **2003**, *92*, 56–63. [CrossRef]
17. Bujacz, A.; Jędrzejczak-Krzepkowska, M.; Bielecki, S.; Redzynia, I.; Bujacz, G. Crystal structures of the *apo* form of β-fructofuranosidase from *Bifidobacterium longum* and its complex with fructose. *FEBS J.* **2011**, *278*, 1728–1744. [CrossRef] [PubMed]
18. Salminen, S.; Endo, A.; Scalabrin, D. Early gut colonization with *Lactobacilli* and *Staphylococcus* in infants: The hygiene hypothesis extended. *J. Pediatr. Gastroenterol. Nutr.* **2016**, *62*, 80–86. [CrossRef] [PubMed]

19. Oliveira, D.L.; Wilbey, R.A.; Grandison, A.S.; Roseiro, L.B. Milk oligosaccharides: A review. *Diary Technol.* **2015**, *68*, 305–321. [CrossRef]
20. Lee, L.Y.; Bharani, R.; Biswas, A.; Lee, J.; Tran, L.-A.; Pecquet, S.; Steenhout, P. Normal growth of infants receiving an infant formula containing *Lactobacillus reuteri*, galacto-oligosaccharides, and fructo-oligosaccharide: A randomized controlled trial. *Matern. Health Neonatol. Perinatol.* **2015**, *1*, 9. [CrossRef] [PubMed]
21. Nguyen, T.T.P.; Bhandari, B.; Cichero, J.; Parakash, S. A comprehensive review on in vitro digestion of infant formula. *Food Res. Int.* **2015**, *76*, 373–386. [CrossRef] [PubMed]
22. Musilova, S.; Rada, V.; Vlkova, E.; Bunesova, V. Beneficial effects of human milk oligosaccharides on gut microbiota. *Benef. Microbes* **2014**, *5*, 273–283. [CrossRef] [PubMed]
23. Orrhage, K.; Nord, C.E. Factors controlling the bacterial colonization of the intestine in breastfed infants. *Acta Paediatr.* **1999**, *88*, 47–57. [CrossRef]
24. Li, M.; Monaco, M.H.; Wang, M.; Comstock, S.S.; Kuhlenschmidt, T.B.; Donovan, S.M. Human milk oligosaccharides shorten rotavirus-induced diarrhea and modulate piglet mucosal immunity and colonic microbiota. *ISME J.* **2014**, *8*, 1609–1620. [CrossRef] [PubMed]
25. McVeagh, P.; Miller., J.B. Human milk oligosaccharides: Only the breast. *Acta Paediatr.* **1997**, *33*, 281–286. [CrossRef]
26. Wallace, T.C.; Marzorati, M.; Spence, L.; Weaver, C.M.; Williamson, P.S. New frontiers in fibers: Innovative and emerging research on the gut microbiome and bone health. *J. Am. Coll. Nutr.* **2017**, *36*, 218–222. [CrossRef] [PubMed]
27. Whisner, C.M.; Martin, B.R.; Schoterman, M.H.; Nakatsu, C.H.; McCabe, L.D.; Wastney, M.E.; van den Heuvel, E.G.; Weaver, C.M. Galacto-oligosaccharides increase calcium absorption and gut *Bifidobacteria* in young girls: A double-blind cross-over trial. *Br. J. Nutr.* **2013**, *110*, 1292–1303. [CrossRef] [PubMed]
28. Weaver, C.M.; Martin, B.R.; Nakatsu, C.H.; Armstrong, A.P.; Clavijo, A.; McCabe, L.D.; McCabe, G.P.; Duignan, S.; Schoterman, M.H.; van den Heuvel, E.G. Galactooligosaccharides improve mineral absorption and bone properties in growing rats through gut fermentation. *J. Agric. Food Chem.* **2011**, *59*, 6501–6510. [CrossRef] [PubMed]
29. Hughes, C.; Davoodi-Semiromi, Y.; Colee, J.C.; Culpepper, T.; Dahl, W.J.; Mai, V.; Christman, M.C.; Langkamp-Henken, B. Galactooligosaccharide supplementation reduces stress-induced gastrointestinal dysfunction and days of cold or flu: A randomized, double-blind, controlled trial in healthy university students. *Am. J. Clin. Nutr.* **2011**, *93*, 1305–1311. [CrossRef] [PubMed]
30. Mussatto, S.I.; Mancilha, I.M. Non-digestible oligosaccharides: A review. *Carbohydr. Polym.* **2007**, *68*, 587–597. [CrossRef]
31. Swennen, K.; Courtin, C.M.; Delcour, J.A. Non-digestible oligosaccharides with prebiotic properties. *Crit. Rev.. Food Sci. Nutr.* **2006**, 459–471. [CrossRef] [PubMed]
32. Juers, D.H.; Heightman, T.D.; Vasella, A.; McCarter, J.D.; Mackenzie, L.; Withers, S.G.; Matthews, B.W. A structural view of the action of *Escherichia coli* (lacZ) β-galactosidase. *Biochemistry* **2001**, *40*, 14781–14794. [CrossRef] [PubMed]
33. Skalova, T.; Dohnalek, J.; Spiwok, V.; Lipovova, P.; Vondrackova, E.; Petrokova, H.; Duskova, J.; Strnad, H.; Kralova, B.; Hasek, J. Cold-active beta-galactosidase from *Arthrobacter* sp. C2-2 forms compact 660 kDa hexamers: Crystal structure at 1.9 Å resolution. *J. Mol. Biol.* **2005**, *353*, 282–294. [CrossRef] [PubMed]
34. Faning, S.; Leahy, M.; Sheehan, M. Nucleotide and deduced amino acid sequences of *Rhizobium meliloti* 102F34 *lacZ* gene: Comparison with prokaryotic beta-galactosidases and human beta-glucuronidase. *Gene* **1994**, *141*, 91–96. [CrossRef]
35. Burchhardt, G.; Bahl, H. Cloning and analysis of the beta-galactosidase-encoding gene from *Clostridium thermosulfurogenes* EM1. *Gene* **1991**, *106*, 13–19. [CrossRef]
36. Rutkiewicz-Krotewicz, M.; Pietrzyk-Brzezinska, A.J.; Sekula, B.; Cieslinski, H.; Wierzbicka-Wos, A.; Kur, J.; Bujacz, A. Structural studies of a cold-adapted dimeric β-D-galactosidase from *Paracoccus* sp. 32d. *Acta Crystallogr. D* **2016**, *72*, 1049–1061. [CrossRef] [PubMed]
37. Pawlak-Szukalska, A.; Wanarska, M.; Popinigis, A.T.; Kur, J. A novel cold-active β-D-galactosidase with transglycosylation activity from the Antarctic *Arthrobacter* sp. 32cB-gene cloning, purification and characterization. *Process. Biochem.* **2014**, *49*, 2122–2133. [CrossRef]

38. Shaw Stewart, P.D.; Kolek, S.A.; Briggs, R.A.; Chayen, N.E.; Baldock, P.F.M. Random microseeding: A theoretical and practical exploration of seed stability and seeding techniques for successful protein crystallization. *Cryst. Growth Des.* **2011**, *11*, 3432–3441. [CrossRef]
39. Bujacz, G.; Wrzesniewska, B.; Bujacz, A. Cryoprotection properties of salts of organic acids: A case study for a tetragonal crystal of hew lysozyme. *Acta Crystallogr. D* **2010**, *66*, 789–796. [CrossRef] [PubMed]
40. Sparta, K.M.; Krug, M.; Heinemann, U.; Mueller, U.; Weiss, M.S. Xdsapp2.0. *J. Appl. Crystallogr.* **2016**, *49*, 1085–1092. [CrossRef]
41. McCoy, A.J.; Grosse-Kunstleve, R.W.; Adams, P.D.; Winn, M.D.; Storoni, L.C.; Read, R.J. Phaser crystallographic software. *J. Appl. Cryst.* **2007**, *40*, 658–674. [CrossRef] [PubMed]
42. Emsley, P.; Cowtan, K. Coot: Model-building tools for molecular graphics. *Acta Crystallogr. D* **2004**, *60*, 2126–2132. [CrossRef] [PubMed]
43. Murshudov, G.N.; Vagin, A.A.; Dodson, E.J. Refinement of macromolecular structures by the maximum-likelihood method. *Acta Crystallogr. D* **1997**, *53*, 240–255. [CrossRef] [PubMed]
44. Winn, M.D.; Isupov, M.N.; Murshudov, G.N. Use of TLS parameters to model anisotropic displacements in macromolecular refinement. *Acta Crystallogr. D* **2001**, *57*, 122–133. [CrossRef] [PubMed]
45. Gerday, C. Psychrophily and catalysis. *Biology* **2013**, *2*, 719–741. [CrossRef] [PubMed]
46. Bujacz, A.; Rutkiewicz-Krotewicz, M.; Nowakowska-Sapota, K.; Turkiewicz, M. Crystal structure and enzymatic properties of a broad substrate-specificity psychrophilic aminotransferase from the Antarcticsoil bacterium *Psychrobacter* sp. B6. *Acta Crystallogr. D* **2015**, *71*, 632–645. [CrossRef] [PubMed]
47. Krissnel, E.; Henrick, K. Interference of macromolecular assemblies from crystalline state. *J. Mol. Biol.* **2007**, *372*, 774–797. [CrossRef] [PubMed]
48. Talens-Perales, D.; Polaina, J.; Marín-Navarro, J. Enzyme Engineering for Oligosaccharide Biosynthesis. In *Frontier Discoveries and Innovations in Interdisciplinary Microbiology*; Springer: New Delhi, India, 2016; Chapter 2; pp. 9–31.